An applicable approach to mitigate pressure rise rate in an HCCI engine with negative valve overlap

Applied Energy 257 (2020) 114018

Contents lists available at ScienceDirect

Applied Energy

journal homepage: www.elsevier.com/locate/apenergy

An applicable approach to mitigate pressure rise rate in an HCCI engine with negative valve overlap

Jacek Hunicz[a,*], Maciej Mikulski[b], Michal S. Geca[a], Arkadiusz Rybak[a]

[a] Lublin University of Technology, Faculty of Mechanical Engineering, Nadbystrzycka 36, 20-618 Lublin, Poland
[b] University of Vaasa, School of Technology and Innovation, Energy Technology, Wolffintie 34, Vaasa FI-65200, Finland

HIGHLIGHTS

- Assessment of various measures to extend load in HCCI with NVO fuel reforming.
- Complex PRR mitigation mechanisms narrowed down to their net phasing effects.
- Late and long combustion is the key primary driver for low PRR.
- Expansion rate and NVO fuel reforming have a secondary effect.
- NVO injection and VVA makes PRR control feasible for HCCI without trade-offs.

ARTICLE INFO

Keywords:
HCCI
Negative valve overlap
Boost
Pressure rise rate
Direct injection

ABSTRACT

Low-temperature combustion in a homogeneous-charge compression-ignition (HCCI) engine offers high thermal efficiency while cutting off emissions. However, HCCI's feasibility is hampered by excessive peak pressure rise rates under high load, causing combustion noise and possible engine damage. This study considers extending the high-load limit in a boosted HCCI engine accommodating variable valve timing and fuel reforming during negative valve overlap. Three techniques are evaluated on a research engine: (i) exhaust valve timing retardation (ii) boost pressure adjustment and (iii) reduction of fuel subjected to reforming. Two load regimes are explored: a mid-load point with indicated mean effective pressure of 0.61 MPa; and high-load conditions achieved by 25% more fuelling. The former is often reported as boundary condition for HCCI's, the latter is usually far beyond the acceptable pressure rise rate limit. Results indicate that strategies (i) and (iii) offer a trade-off-free solution for high-load extension. This can be realized as a supervisory, in-cylinder pressure based, control function. Independently of the pressure rise rate mitigation method considered, two key variables are crucial for closed-loop control: the in-cylinder volume at 50% fuel burnt and the combustion duration. They are closely coupled and can be real-time calculated using well-established control framework based on sensing the combustion timing. The expansion rate and differences in fuel mass subjected to reforming are secondary for pressure rise rate estimation and should be considered if greater accuracy is required.

1. Introduction

Reducing the environmental impact of motor vehicles and industrial machinery powered by combustion engines is a global challenge. It demands ever-greater focus on improving energy efficiency and reducing exhaust emissions. The most problematic exhaust components are nitrogen oxides (NO_X) and particulate matters (PM) [1]. Health and environmental concerns about both of these have led to a marked decline in the use of diesel engines in cars. It should be noted however that bad reputation of diesel engines is largely fuelled by a certain trust crisis and does not fully represent the current state of the art in this technology.

Abbreviations: CAX, crank angle of X% MFB; DI, direct (fuel) injection; EGR, exhaust gas recirculation; EVC, exhaust valve closing; HCCI, homogeneous charge compression ignition; HRR, net heat release rate; IMEP, indicated mean effective pressure; IVC, intake valve closing; IVO, intake valve opening; LHF, lower heating value (of the fuel); LTC, low temperature combustion; MAP, manifold (intake) absolute pressure; m_F, mass of fuel; MFB, mass fraction burned (of the fuel); NO_X, nitrogen oxides; NVO, negative valve overlap; p, in-cylinder pressure; PM, particulate matters; PRR, pressure rise rate; PVO, positive valve overlap; TDC, top dead centre (of the piston); V, instantaneous cylinder volume; γ, ratio of specific heats

* Corresponding author.
E-mail address: j.hunicz@pollub.pl (J. Hunicz).

https://doi.org/10.1016/j.apenergy.2019.114018
Received 3 June 2019; Received in revised form 31 August 2019; Accepted 14 October 2019
Available online 24 October 2019

Advanced, low-temperature combustion (LTC) can help eliminate both NO_X and PM from exhaust gases almost completely. LTC in a homogeneous-charge compression-ignition (HCCI) engine is cutting-edge technology offering clean combustion in parallel with high thermal efficiency. The low temperature that prevents NO_X formation is achieved via volumetric combustion of a highly diluted mixture which also gives a smokeless exhaust [2]. Furthermore, a combination of HCCI and advanced biofuels can provide fully sustainable propulsion [3].

However, commercial feasibility of HCCI technology is hampered by excessive peak pressure rise rates (PRR_{max}) and the resulting combustion noise [4–6]. Another hurdle to be overcome is the lack of the direct ignition control [7,8] that conventional spark or compression-ignited engines have. HCCI's auto-ignition is spontaneous and governed by mixture reactivity and temperature conditions [9,10]. In other words, thermodynamic conditions and chemical composition of the combustible mixture at intake valve closing (IVC) define the timing and duration of subsequent combustion process. Some additional controllability after IVC can, however, be introduced by means of direct injection (DI) of fuel, providing mixture stratification [11,12], or by so-called spark assist technology [9,13].

One promising method of achieving controllable HCCI combustion is to use negative valve overlap (NVO), where exhaust re-compression is created between advanced exhaust valve closing (EVC) and intake valve opening (IVO) events. This traps combusted gas inside the cylinder, providing internal exhaust gas recirculation (EGR). Using NVO makes it possible to achieve auto-ignition temperatures of high-octane number fuels like gasoline but under low compression ratios typical of spark-ignition engines [2,14]. It also has been demonstrated that HCCI combustion using NVO exerts a self-stabilization mechanism which relies on coupling thermal conditions between subsequent cycles [15,16]. Engine operation range in NVO mode is, however, limited by the admission of large amounts of residual exhaust gases which reduce air aspiration. Therefore, practical application of HCCI with NVO also needs variable valve actuation (VVA), with NVO operation in partial-load regime, gradually switching to positive valve overlap (PVO) and spark-ignition operation at higher loads [17]. Nevertheless, the extension of the HCCI operating range can reduce overall emissions and improve engine thermal efficiency. Although the issue of reduced aspiration can be mitigated by boosting (turbocharging or supercharging) the high-load operation boundary is still constrained by excessive PRR_{max} [18]. This issue is characteristic for volumetric type of combustion, which is by nature a very rapid process, and controlling it is considered by far the most important challenge for LTC technology.

The following paragraphs give a synthetic review of progress to reduce PRR_{max} by way of clever HCCI combustion control. Most of the studies have focused on exploring one of three techniques:

Increasing charge dilution by use of excess air or EGR.
Introducing mixture stratification by means of late DI.
Altering the mixture's reactivity by fuel blending or reforming.

The first method mainly has been explored for conventional HCCI with PVO and port gasoline injection, where an external heat source gives sufficiently high intake temperatures for auto-ignition during compression. With such a setup, Kulzer et al. [19,20] investigated the effect of charge dilution with excess air on HCCI combustion. Dilution was achieved by increasing the boost pressure from naturally aspirated conditions to as much as 3 bars. The start of combustion was kept at the assumed set point with increased intake temperature. The authors observed simultaneous reduction of PRR_{max} and NO_X emissions, without any trade-off on specific fuel consumption.

The experiments of Dec and Yang [21] aimed to demonstrate the highest engine-load for boosted HCCI operation with external EGR, without hampering the adopted PRR_{max} and peak pressure limits. The maximum attainable load (indicated mean effective pressure – IMEP) was 8.8 bar for lean operation without EGR. With the same constraints, the maximum load extended to almost 16 bar IMEP while applying high boost pressure and external EGR.

Interestingly, although these examples of HCCI research found it was possible to reduce PRR with large amounts of excess air derived from boosted engine operation, other studies produced contrary results. For instance, both Yap et al. [22] and Canakci [23] used similar experimental setups as Kuzler et al. [20] but reported excessive PRR_{max} increase with elevated intake pressure. Scaringe et al. [18] reported the same trend for lean HCCI operation and proved that PRR-limited load range could not be extended with alternative mixture dilution measures, such as EGR. The recent work by Shingne et al. [24] uses reactive computational fluid dynamics simulations and quasi-dimensional modelling to attempt to explain why raising intake pressures leads to increased PRR_{max}. The authors prove that high boost reduces the heat (per unit charge mass) transferred to cylinder walls. This results in significantly faster combustion, which ultimately was the primary reason for increased PRR_{max} under boosted operation. This simulation study was not able to confirm the possibility of actually increasing the HCCI load range by application of boost, as found in the experimental studies by Kulzer et al. [20] and Dec and Yang [21]. Still it revealed the importance of in-cylinder thermal stratification as one of the PRR_{max} control methods in HCCI.

Additional thermal and chemical stratification can be introduced as a control measure for HCCI engines, by means of DI. When a fraction of the total fuel value is injected late during the compression stroke, there is insufficient time for it to mix completely with the remaining in-cylinder fluid before combustion commences. Furthermore, DI of liquid fuel enhances thermal stratification and reduces the bulk temperature by means of evaporative cooling effect.

For a PVO HCCI concept, Dec et al. [25] introduced an additional gasoline DI to the already existing port fuel injection system, aiming to achieve partial stratification of the in-cylinder charge. The authors observed a systematic reduction in the PRR_{max} while increasing the ratio of directly injected fuel. The phenomenon was attributed to elongated combustion due to the introduced stratification. Note however that the effect manifested solely for very lean operation at high boost pressures. Towards stoichiometric conditions, changing the split ratio had almost no effect on the recorded PRR_{max}.

In their HCCI development research Turkcan et al. [26,27] studied the effect of DI timing on combustion, engine efficiency and emissions. In this study, fuel injection was split into two portions, with 80% of the fuel was injected early during the intake phase and the remaining 20% was injected directly during the compression stroke. Increase of stratification via delaying the start of injection (SOI) of the second injection effectively reduced PRR_{max}, but increased exhaust-gas opacity. Work by Hunicz et al. [28], extended the scope of research towards the effects of fuel stratification by examination of different split ratios and a broad range of excess-air ratios. Abstracting from the specifics of HCCI operating conditions, the general conclusion was that fuel stratification is an effective measure to reduce simultaneously NO_X emissions and PRR. At the same time, the results confirmed a clear trade-off between the PRR/NOx emission on one side and CO/HC and soot emission on the other.

Yang et al. [29] tailored their DI HCCI experiments to decouple the effects of compositional stratification from the thermal effects of fuel evaporation. To achieve this, the authors used (for stratification) gasoline and methanol – fuels that are characterized by qualitatively different reactivity and heat of vaporization. An important conclusion was that the thermal effects are far more important compared to those of compositional nature. Confirmation of this observation for mono-fuel gasoline HCCI was provided experimentally by Kodavasal et al. [30].

In terms of altering mixture reactivity as a method to control PRR and combustion phasing in an LTC engine, the majority of recent works focused on in-cylinder blending of two fuels with extremely different properties. This type of LTC is commonly referred to as reactivity controlled compression ignition (RCCI). It has been demonstrated to

show full-load capability with superior efficiency and ultra-low NO_X emissions, using a variety of fuels including: gasoline-diesel [31,32], ethanol-diesel [33] and natural gas-diesel [34,35]. Despite promising results on heavy-duty platforms, the dual-fuel concept lacks feasibility for future hybridized light-duty applications. For similar reasons, related to system complexity and sizing, various concepts of on-board fuel reforming using external reactors will not be discussed in detail here. For more information regarding LTC load extension potential with such technology, the reader is referred to a recent work by Asai et al. [36].

Another method of altering mixture reactivity in single-fuel HCCI combustion is via early fuel injection during the NVO period. When the temperature of the recompressed exhaust gases is sufficiently high, the injected fuel undergoes chemical reactions to produce species with different reactivity. They are retained in the cylinder through the next main compression cycle and influence the auto-ignition properties of the air-fuel mixture. Substantial research over recent years has focused on understanding how NVO fuel injection actually affects the main combustion event. For instance, Yu et al. [37] and Xie et al. [38] identified the species that are present in the gasoline-reforming mechanism and that have a profound impact on promoting auto-ignition. These include ethane, ethylene, formaldehyde, methanol and acetylene. The authors concluded that acetylene, despite its low concentrations in the reformed gases, has a dominant effect. Puranam and Steeper [39] confirmed this hypothesis by means of a controlled experiment where acetylene was added in small quantities to isooctane-air mixture. More recently, researchers from the University of Minnesota managed to correlate trends in start of combustion with concentrations of different gasoline-reforming products [40,41]. The latest work by Hunicz and Mikulski [10] focused on understanding the thermal effects of NVO fuel injections on HCCI combustion. The authors prove that thermal effects dominate chemical phenomena in terms of influencing combustion when the engine is operated at lean mixture conditions. Importantly, it is possible to achieve superior control of combustion-phasing in such a system by adjusting both the NVO start of injection and the split ratio, thereby balancing the thermal effects.

The follow-up studies by the authors have built on this new route for controllable HCCI in an engine using NVO by exploring the maximum attainable engine-load before it is restricted by permissible PRR level and acceptable emissions levels. One of their findings is that the simultaneous appearance of thermal and compositional stratification results in a non-linear effect of late gasoline injection on auto-ignition advance and combustion duration. Namely, thermal stratification created at earlier fuel injection in the compression stroke delays auto-ignition, whereas compositional stratification occurring at later injection advances the start of combustion [42]. Additionally, reduction of the reaction rate can be achieved solely for larger amounts of fuel injected for stratification. Studies performed showed that the substantial effect on PRR was observed beyond the threshold of stratification that promotes PM production [28,43].

The picture of PRR mitigation in HCCI emerges from the above-mentioned studies as a complex non-linear problem. Some aspects of the individual parameters' influence are not yet fully understood: witness the conflicting effects of boost pressure on PRR_{max} reported in different studies. While VVT and DI provide PRR mitigation in residually affected combustion they also add complexity. This is the reason why multi-input, PRR-oriented control has not been demonstrated for HCCI with NVO fuel reforming. This is despite its potential to significantly extend HCCI load capability in practical implementation, contributing to better overall performance.

The present work aims to tackle this gap between fundamental-level research into individual parameters' influence on combustion harshness and its application by means of control development. This is pursued through attempting to narrow down the multi-parameter PRR mitigation problem by correlating it to typical indicators used in combustion control, namely crank angle (CA) of 50% mass burned and combustion duration. Measures explored to widen HCCI's high-load regime include variable mixture temperature and composition, combined with controlled reactivity. To this end, mixture composition and thermodynamic state are controlled via variable EVC timings and boost pressure. Mixture reactivity is controlled by the amount of fuel subjected to reforming by its injection early during the NVO period.

2. Object and methods.

2.1. Experimental facility

A 4-stroke, single-cylinder engine with VVA is the research object in this study. To achieve HCCI combustion using NVO, variable valve-lift is achieved hydraulically [44]. The engine's displaced volume is 498.5 cm^3 and its geometrical compression ratio of 11.7 is typical for a spark-ignition engine. The combustion chamber is located in a bowl-shaped engine head. The piston face is generally flat but with a slight protruding perimeter to generate some squish as the piston approaches TDC. Fuel is delivered directly to the cylinder using a side-mounted, swirl-type, single-stream Bosch HDEV electromagnetic injector. The injector is positioned tangentially to the intake port-generated swirl and inclined by 38° with respect to the cylinder axis. Detailed specification of the research engine is provided in Table 1. All the crank-angle-based values are given as after TDC during the NVO period.

The engine is coupled with direct current dynamometer. The test stand includes a complete automation system with accurate conditioning of cooling liquid and oil temperatures. The intake system is equipped with a vane compressor powered by an alternating current motor cooperating with a frequency converter. The compressor maintains constant pressure of the intake air. Intake air temperature is conditioned by a heat exchanger cooled or heated by water to single degree point accuracy. The schematic diagram of the test stand is shown in Fig. 1.

The engine test stand is equipped with all measurement devices required for completion of the planned tests. The measurement system consists of an intake-air mass-flow meter, a fuel balance and a set of pressure and temperature transducers for measuring intake and exhaust thermodynamic conditions. Exhaust gas composition is measured with the Fourier transform infrared (FTIR) analytical system from AVL. The excess air ratio (λ) is measured by a Bosch LSU 4.2 oxygen sensor and an ETAS LA4 lambda meter for redundancy. The thermodynamic analyses are based on the in-cylinder pressure signal. This is measured by a GH12D miniature pressure transducer from AVL, installed directly in the engine head and connected via a charge amplifier to the test bench acquisition system. An optical encoder with a 0.1 °CA resolution triggers the high-speed pressure data. The PC-based engine control system uses dedicated in-house software and is connected to a timing module which controls the injection timing, duration and spark generation. This last function is used in this research solely to initiate autonomous HCCI operation during engine startup and warm-up phase.

2.2. Experimental conditions, procedure and data analysis

The current experiments explore HCCI combustion at two engine-load conditions: at a threshold PRR and at beyond an acceptable level

Table 1
Research engine specifications.

Parameter name	Value
Displaced volume	498.5 cm^3
Bore	84 mm
Stroke	90 mm
Compression ratio	11.7
No of valves	2
Fuel injector	Single stream, side mounted
Boost device	Vane compressor, electrically driven

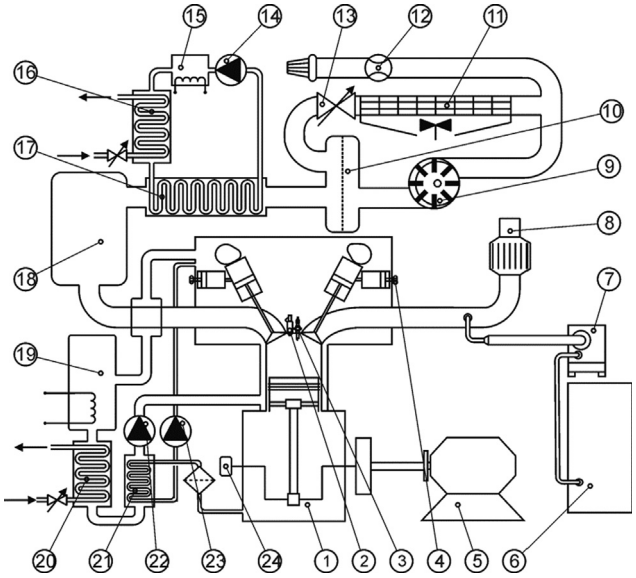

Fig. 1. Schematic diagram of the single-cylinder engine test stand; (1) engine, (2) fuel injector, (3) spark plug, (4) valve lift adjuster, (5) dynamometer, (6) exhaust gas analyser, (7) heated filter, (8) exhaust runner, (9) vane compressor, (10) intake plenum/oil separator, (11) air cooler, (12) air mass flow meter, (13) air by-pass valve, (14–17) intake air temperature conditioning system, including: pump, electric heater and heat exchangers, (18) intake plenum, (19–23) engine coolant and oil conditioning system, including: pumps, electric heater and heat exchangers, (24) crankshaft encoder.

PRR. Accordingly, two fixed-total fuel quantities are applied, approximately 19 mg and 24 mg, providing net IMEP levels of approximately 0.61 MPa and 0.75 MPa. The lower engine-load point was determined in earlier research to be a borderline of acceptable combustion harshness [45]. The two selected load levels are referred to as mid-load and high-load operation throughout this study. The engine's rotational speed is held constant at 1500 rpm. Fuelling is with European Euro Super, commercial gasoline with a research octane number of 95. Fuel is injected directly into the cylinder in two doses. The first start-of-fuel injection (SOI_1) is set to −40 °CA (40 °CA before TDC in the NVO period) and the second injection (SOI_2) commences at 90 °CA. The timing of SOI_1 is based on earlier works [46,47] and selected because it provided the highest production of reactive species that are identified as auto-ignition promoters. It should be noted that the investigated engine is unable to operate in autonomous HCCI mode with boost but without the early NVO injection. This is because applying boost reduces the IVC temperature significantly. Exhaust-fuel reactions from early NVO injection counter this by providing additional heat and combustion-promoting species to the charge, thus enabling auto-ignition at the end of compression. The timing of the second fuel injection at the beginning of intake process is intended to create close to homogenous charge conditions in the cylinder. It is assumed that all fuel would vaporize and mixture temperature would be equalized before the IVC. In other words, the fuel state change does not affect compression temperature histories.

The study investigates the combination of three potential measures to reduce PRR and thus extend the high-load range of engine operation in HCCI mode. To this end, three parameter sweeps are performed: (i) intake manifold absolute pressure (MAP) from 140 kPa to 180 kPa, (ii) EVC timing from −80 °CA to −68 °CA, (iii) split-injection ratio between the first and second injection. Here, the amount of fuel injected with SOI_1 is varied from approximately 5.8 mg down to the smallest quantity limited by either injector capability or misfires (approximately 2 mg). Detailed information on the control parameters used to characterize the combustion is provided in Table 2. Valve-lift profiles and injection timings are visualized in Fig. 2. Note that intake-valve timing

Table 2
Engine operation parameters.

Parameter name	Value	
Rotational speed	1500 rpm	
SOI_1	−40 °CA,	
SOI_2	90 °CA	
IVO	83 °CA	
IVC	213 °CA	
EVO	521 °CA, 527 °CA, 533 °CA	
EVC	−80 °CA, −74 °CA, −68 °CA	
MAP	140 kPa, 160 kPa, 180 kPa	
Coolant temperature	90 °C	
Intake air temperature	30 °C	
Fuel rail pressure	10 MPa	
Condition name	Mid-load	High-load
Total fuel value	19 mg	24 mg
Mass of NVO fuel	2.14 mg…5.79 mg	2.02 mg…5.75 mg
Net IMEP	0.61 MPa*	0.75 MPa*

*IMEP is not explicitly controlled – slight variations around this value from point to point are observed due to differences in indicated efficiency.

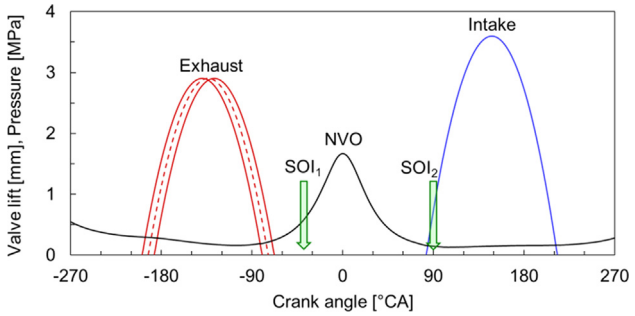

Fig. 2. Valve-lift profiles, SOI locations against an exemplary in-cylinder pressure during gas exchange and NVO.

is intentionally kept constant to provide the same thermodynamic compression ratio for all conditions.

The in-cylinder pressure analysis is based on the first law of thermodynamics. The net heat release rate (HRR) is calculated using the following formula

$$\mathrm{HRR} = \frac{\gamma}{\gamma - 1} p \cdot \Delta V + \frac{1}{\gamma - 1} V \cdot \Delta p \tag{1}$$

where finite steps of volume (V) and pressure (p) were calculated every 0.1 °CA. The ratio of specific heats (γ) is calculated based on the instantaneous temperature and composition of the in-cylinder mixture. The volume-averaged temperature is calculated using the gas equation of state with consideration of the effect of mixture composition on the gas constant. The same procedure is applied for the NVO period. The mass fraction burned (MFB) functions are calculated on the basis of cumulative heat release. Locations of characteristic points defining combustion advance, i.e. 5%, 50% and 95% MFB are read from MFB curves and denoted as CA05, CA50 and CA95 respectively, as shown in Fig. 3. Combustion duration is calculated as the distance between CA05 and CA95 and denoted as CA05-95. PRR is calculated as a gradient of linear fitting to the single degree section of the pressure signal (Fig. 3). This is done to reduce the effect of measurement noise on calculated PRR values. The peak PRR (PRR_{max}) values are used as combustion harshness indicators. Note that all the calculations are realized on the individual cycle basis. Presented curves of pressure, temperature and HRR are the ensemble averages from 100 cycles. Similarly, all combustion timing parameters and PRR_{max} values are averages from 100 consecutive combustion events.

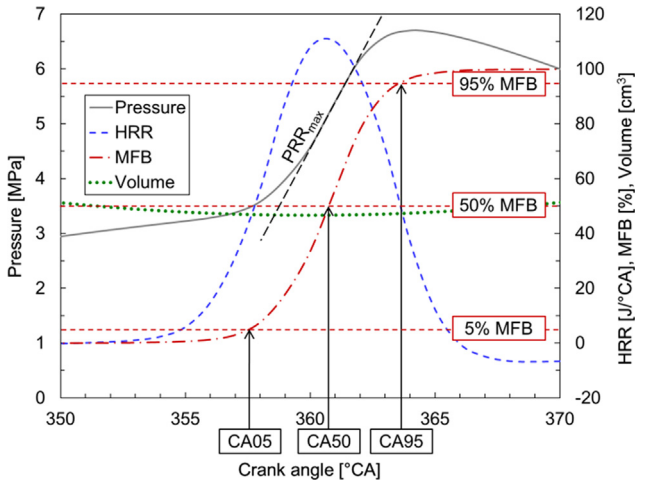

Fig. 3. Exemplary in-cylinder pressure with calculated HRR and MFB functions. The definitions of analysed combustion parameters are also introduced in the figure.

2.3. Theoretical background for PRR data analysis

Abstracting from the direct measurement method for determining the PRR as outlined above for analytical purposes, let us consider an alternative way of estimating this combustion indicator. The in-cylinder pressure change resulting from the combustion can be analytically derived from the first law of thermodynamics. Manipulating Eq. (1) gives:

$$\Delta p = \frac{1}{V}[\mathrm{HRR}(\gamma - 1) - \gamma \cdot p \cdot \Delta V] \tag{2}$$

Scaringe et al. [18] demonstrated that the cumulative heat release process can be considered almost linear for volumetric-type combustion. This is clearly seen for a typical HCCI case, on the MFB plot in Fig. 3. If the heat and combustion losses are further neglected, as very small terms, during fast HCCI combustion, HRR can be estimated as:

$$\mathrm{HRR} \approx \frac{m_F \cdot \mathrm{LHV}}{\mathrm{CA05} - 95} \tag{3}$$

where m_F is the fuel mass, which together with the lower heating value (LHV), gives the total energy introduced into the cylinder. Because HCCI combustion is rather quick and happens around the TDC, where ΔV is nearly zero, as evident from Fig. 3, the expansion term in Eq. (2) can also be neglected. Further examination of Fig. 3 shows peak PRR falls close to the CA50 for a typical HCCI case. Considering the above-mentioned angular insensitivity around TDC, the cylinder volume value at this particular CA can be used in Eq. (2) to arrive at PRR_{max}. Considering all the above assumptions, and disregarding the CA dependency of γ, one finally gets:

$$\mathrm{PRR}_{max} \approx \frac{(\gamma - 1) \cdot m_F \cdot \mathrm{LHV}}{V(\mathrm{CA50}) \cdot (\mathrm{CA05} - 95)} \tag{4}$$

Eq. (4) can be used to provide the uniform explanation of the effects exerted on PRR_{max} by different air-path and fuelling strategies investigated in this paper. Ultimately, it provides the starting point for narrowing down the multi-parameter PRR mitigation problem, necessary from the perspective of applied HCCI with NVO fuel reforming, thus enabling the corresponding discussion in Sections 3.3 and 3.4.

3. Results and discussion

The main assumptions for the HCCI process are a fully premixed charge and spontaneous volumetric combustion. Thus, thermodynamic conditions of the charge at IVC and mixture reactivity determine the moment of auto-ignition and combustion rates, which in turn affect PRR. In engines using trapped residuals to enable HCCI combustion, the thermal processes during the NVO period are largely responsible for shaping IVC conditions.

The discussion of results is arranged to facilitate this cause-to-effect structure. First is elaboration of the effects of the individual air-path (Section 3.1). Then comes discussion about the influence of fuelling strategies on mixture composition and thermodynamic state (IVC conditions), including consideration of thermal effects manifesting during NVO (Section 3.2).

The following Section 3.3 aims to synthesize the lessons learned through the detail analysis of the individual combustion harshness-reduction measures. These are put into perspective by Eq. (4), providing a systematic explanation of the trends observed in PRR_{max}. Those are correlated to typical indicators used in combustion engine control to support practical implementation in embedded systems. The discussion concludes in Section 3.4 with an outlook on applicability of the investigated HCCI load extension measures, supported by a trade-off analysis (efficiency and NO_X emissions).

3.1. Mixture composition and thermodynamic state: air-path effects

To facilitate further discussion on combustion timings and rates, Figs. 4–7 provide insight on how the investigated air-path control parameters (boost pressure and exhaust valve timings) affect the mixture state. This is illustrated at both load regimes while injecting nearly the same amount of fuel (approximately 3.3 mg) during NVO.

Increasing the intake pressure improves the air aspiration and thus increases excess air ratio but it has a trivial effect. Aside from this, Fig. 4 reveals important information on the effect of EVC timing on λ. Retarding the EVC reduces the amount of trapped residuals, which ultimately promotes fresh-air aspiration. For instance, the EVC sweep from −80 °CA to −68 °CA at MAP = 160 kPa increases λ from 1.37 to 1.48 and from 1.22 to 1.3 for the mid- and high-load cases respectively.

Fig. 5 shows the range of EGR ratio that is controlled both by EVC timing and by boost pressure. The first effect is straightforward, because the amount of trapped residuals is metered directly by the EVC. Thus, the later the EVC event, the lower the amount of the re-breathed exhaust. Additionally, reducing the amount of trapped residuals enhances fresh-air aspiration, further contributing to the reduction in EGR rate. Furthermore, the increase of MAP, and thus the amount of aspirated air, also reduces EGR. This effect is to some extent hindered by the reduction in exhaust temperature associated with elevated MAP, as shown in Fig. 6. The temperature affects exhaust gas density, and thus the amount of trapped residuals.

For all measurement points in Fig. 5 the EGR ratio varies between 36% and 38% for the mid-load case (fuel quantity of 19 mg) and from 31% to 36% for the high-load case. The smaller change in EGR, observed when lower fuel values are used, is associated with the NVO thermal phenomenon whereby the increase of oxygen content in the trapped residuals enhances heat release during the NVO period. As a result, IVO temperature is elevated and fresh-air aspiration restricted, reducing the effect of MAP. In the case of higher fuel quantity, the amount of oxygen available during the NVO period is lower. Thus, the

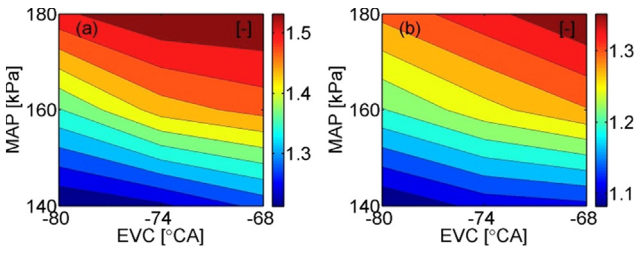

Fig. 4. Excess-air ratio versus MAP and EVC timing at $m_{FNVO} \approx 3$ mg; (a) mid-load, (b) high-load.

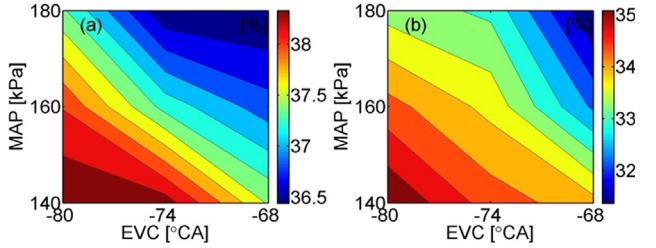

Fig. 5. EGR rate versus MAP and EVC timing at $m_{FNVO} \approx 3$ mg; (a) mid-load, (b) high-load.

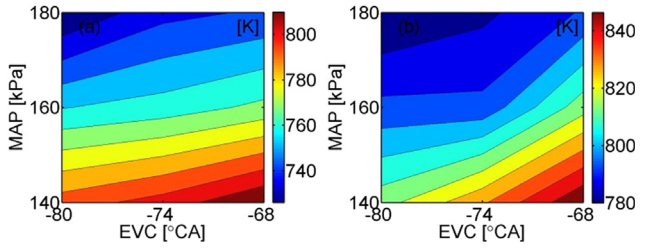

Fig. 6. Exhaust temperature versus MAP and EVC timing at $m_{FNVO} \approx 3$ mg; (a) mid-load, (b) high-load.

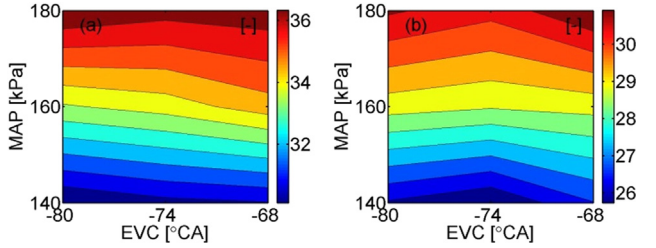

Fig. 7. Overall fuel dilution versus MAP and EVC timing at $m_{FNVO} \approx 3$ mg; (a) mid-load, (b) high-load.

effect of MAP on the EGR rate is damped by the NVO heat release to a much smaller extent than in the mid-load case.

The discussed trade-off between the excess air and the EGR gives an almost constant overall fuel dilution (defined as cumulative mass of air and exhaust related to mass of fuel) while changing the EVC, as shown in Fig. 7. Under investigated conditions, the increase in the mass of trapped residuals with EVC advance is compensated by the reduction of intake air mass flow. Consequently, the fuel dilution by air and exhaust is affected solely by intake pressure.

Interestingly, Fig. 6 shows that exhaust temperature is not only affected by the fuel dilution but also by exhaust valve timing. Furthermore, the trend contradicts expectations based on engine-cycle analysis. Early EVO is expected to increase the temperature at the expense of indicated work but actually the exhaust temperature drops with advanced valve timing. This peculiar effect is attributable to the influence of valve actuation on combustion timing because the reduction of the amount of trapped residuals, associated with later EVC (Fig. 5) delays the combustion.

Figs. 8 and 9 provide detail explanation of the effect of EVC on thermodynamic conditions discussed in Figs. 5–7. Fig. 8a shows that NVO compression temperature drops while retarding the EVC (from −80 towards −68), whereas Fig. 6a shows a corresponding increase of exhaust temperature. Note however, that the NVO thermodynamic compression ratio decreases with EVC delay. As a result, the trend in exhaust temperature is mirrored.

Comparison of Fig. 8a and 8b shows clearly that the thermal effects of fuel reforming are very strong in the mid-load case and largely insensitive to EVC timing. This is clearly seen in Fig. 9. Here, the

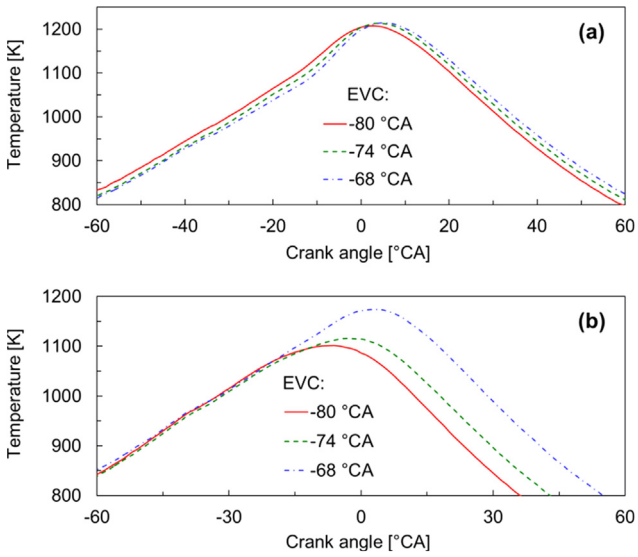

Fig. 8. In-cylinder temperature during the NVO period for different EVC timings at MAP = 160 kPa and $m_{FNVO} \approx 4$ mg; (a) mid-load, (b) high-load.

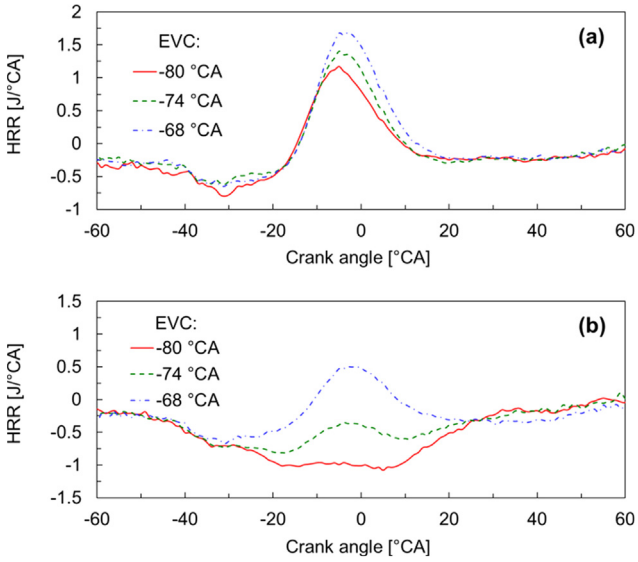

Fig. 9. Net heat release rate during the NVO period for different EVC timings at MAP = 160 kPa and $m_{FNVO} \approx 4$ mg; (a) mid-load, (b) high-load.

differences in HRR levels during NVO stem from different λ values, i.e. availability of oxygen. For the mid-load case, while retarding EVC with unchanged overall fuel dilution (Fig. 7a) the higher oxygen content stemming from less EGR (Fig. 5a) enables more fuel reformation, which ultimately increases the HRR (Fig. 9a). This leads to the observed increase in the IVO in-cylinder temperature (Fig. 8a), and finally, restricted air admission, as shown in Fig. 7a.

For the high-load case in Fig. 9b, the HRR is more sensitive to exhaust valve timing because with the higher (23 mg) overall fuel value there is less oxygen in the trapped residuals. For the earliest EVC timing of −80 °CA, as an extreme example, the main event mixture is nearly stoichiometric so there is not enough oxygen in the exhaust to trigger exothermal reactions during NVO. Still, despite the quantitative difference, the trends in NVO HRR and in-cylinder temperature (Fig. 8b) associated with valve timing are qualitatively the same as in the mid-load, 19 mg fuel case discussed earlier.

Figs. 10 and 11 present the NVO in-cylinder temperature and HRR for the three tested MAP conditions. They all represent an exemplary case with NVO fuel value and EVC in the middle of the explored range:

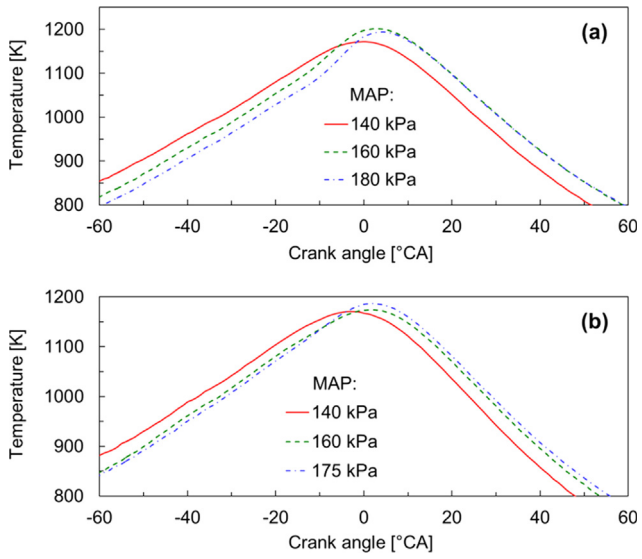

Fig. 10. In-cylinder temperature during the NVO period for different boost pressures at EVC = −74 °CA and $m_{FNVO} \approx 3$ mg; (a) mid-load, (b) high-load.

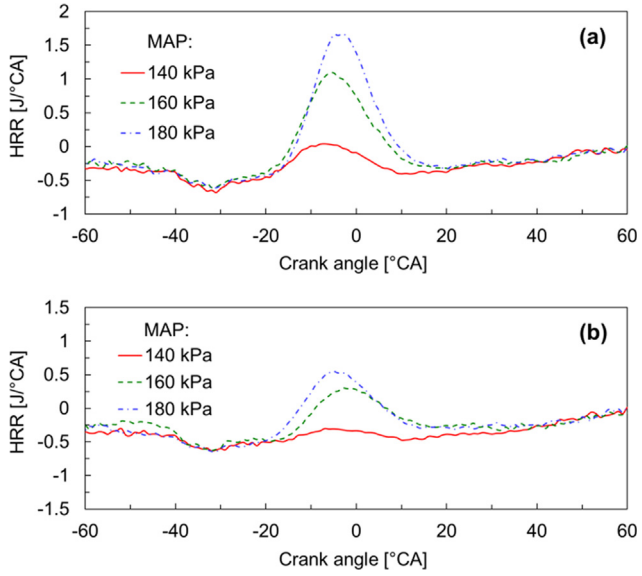

Fig. 11. Net heat release rate during the NVO period for different boost pressures at EVC = −74 °CA and $m_{FNVO} \approx 3$ mg; (a) mid-load, (b) high-load.

3 mg and −74 °CA respectively. Here the trends in HRR (Fig. 11) correspond to the increased oxygen content with increasing MAP and thus, share the same explanation as given in discussed valve timing sweep. The NVO compression temperature in Fig. 10, on the other hand, corresponds clearly to the trend in the exhaust temperature in Fig. 5, which tends to reduce with overall leaning of the mixture associated with increased MAP. The balancing effect of fuel dilution and heat release on IVO temperature is evident in a comparison of Figs. 10 and 11. It is evident from Fig. 10 that the IVO temperature is elevated at higher boost pressures, which ultimately explains the damping effect of NVO fuel reforming on the MAP- λ characteristics. The higher NVO HRR for the mid-load case (Fig. 11a) compared with the high-load case (Fig. 11b) also explains why the noted change in EGR (Fig. 5) is considerably less for smaller fuel quantities. Simply put, the effect of MAP on the EGR rate is significantly damped by the NVO heat release in this particular case.

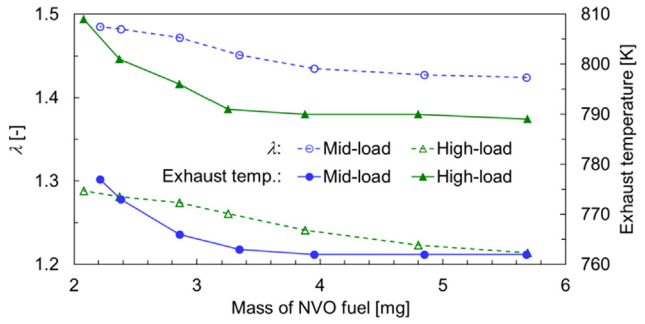

Fig. 12. Excess air ratio and exhaust temperature versus m_{FNVO} at EVC = −74 °CA and MAP = 160 kPa.

3.2. Mixture composition and thermodynamic state: fuel injection effects

The effects of NVO fuel quantity on mixture properties, at exemplary air-path settings: EVC = −74 °CA and MAP = 160 kPa, are shown in Fig. 12. Interestingly, exhaust temperature increases with the reduction of NVO fuel quantity, despite the increase of excess air. As with the EVC effect discussed in Section 3.1, this temperature increase can be attributed to the delayed combustion as well as to the variability in the amount of heat released during the main event combustion. With the constant overall fuel quantity at the given load point, the reduction of the NVO fuel dose acts in favour of the increased heat release during the main event. Fig. 14 provides more insight about this phenomenon. Changes in the EGR ratio resulting from the NVO fuel sweep are the direct consequence of the trends in exhaust temperature and main event λ. At reduced NVO fuel value, both higher exhaust temperature and improved aspiration contribute to the reduction of EGR.

Figs. 13–17 provide the necessary level of detail to understand the influence of NVO fuel quantity on lambda and overall mixture conditions. This is discussed by means of thermal effects at NVO (Figs. 13 and 14) and main cycle combustion characteristics (Figs. 15–17). Comparing Fig. 13a and b shows that although the trends in exhaust temperature are generally the same (see Fig. 12), the effect of NVO injection in both load cases is qualitatively different. At mid-load (Fig. 13a), the increase in NVO fuel value elevates the temperature of the recompressed exhaust gases while at high-load (Fig. 13b) the effect is non-monotonic, with the highest fuel value resulting in significant

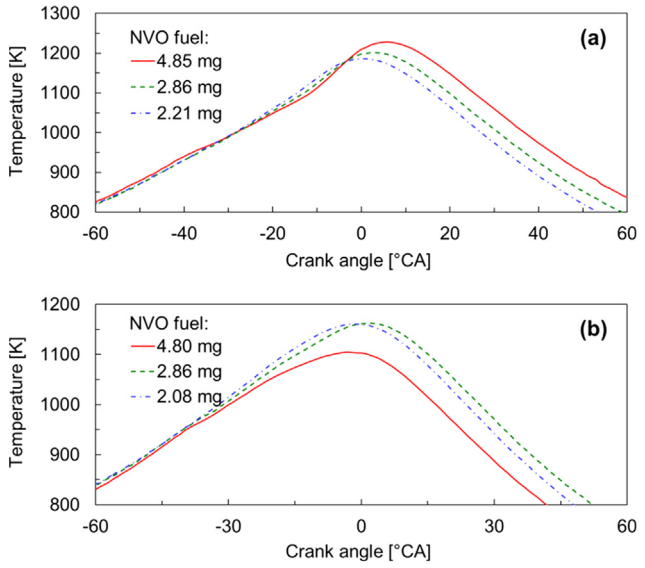

Fig. 13. In-cylinder temperature during the NVO period for different quantities of NVO fuel at EVC = −74 °CA and MAP = 160 kPa; (a) mid-load, (b) high-load.

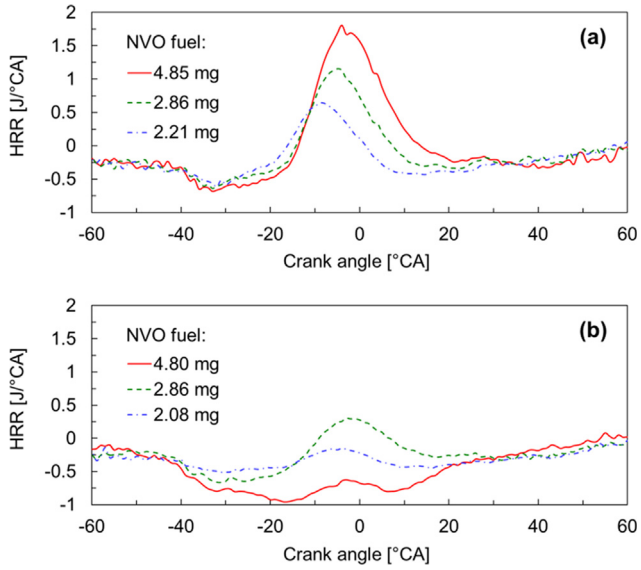

Fig. 14. Net heat release rate during the NVO period for different quantities of NVO fuel at EVC = −74 °CA and MAP = 160 kPa; (a) mid-load, (b) high-load.

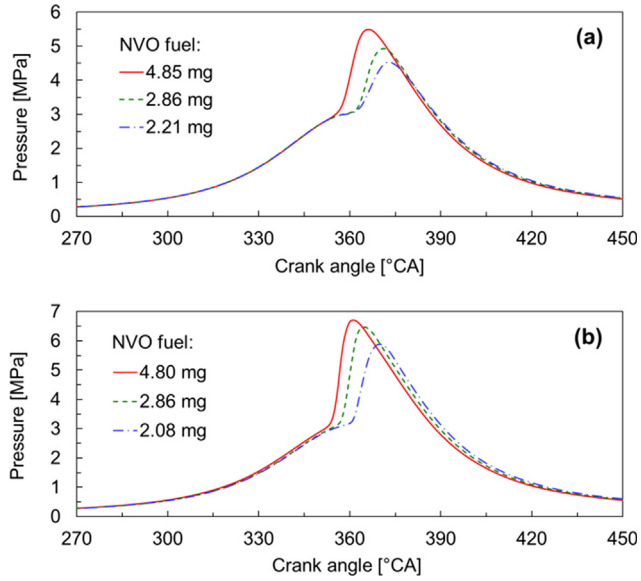

Fig. 15. In-cylinder pressure during the main event for different quantities of NVO fuel at EVC = −74 °CA and MAP = 160 kPa; (a) mid-load, (b) high-load.

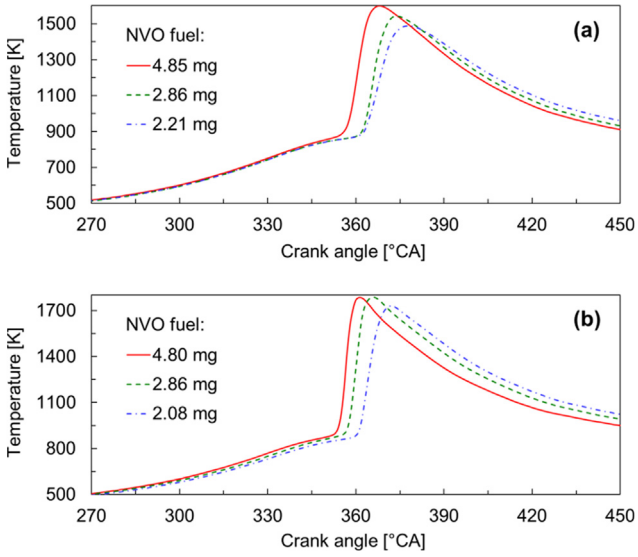

Fig. 16. In-cylinder temperature during the main event for different quantities of NVO fuel at EVC = −74 °CA and MAP = 160 kPa; (a) mid-load, (b) high-load.

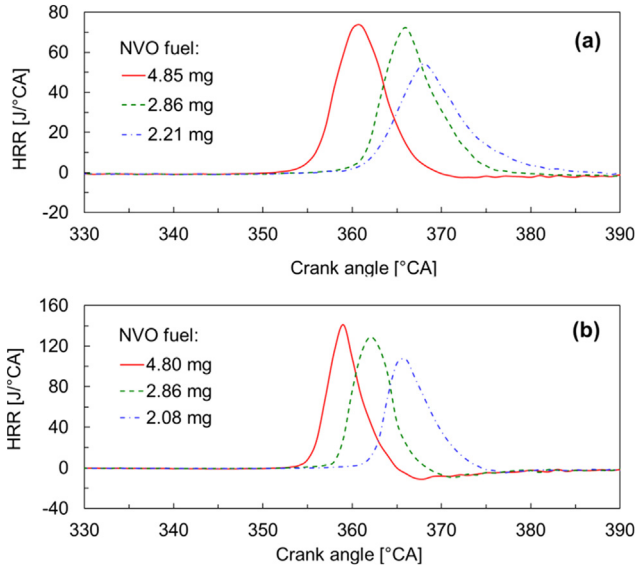

Fig. 17. Heat release rate during the main event for different quantities of NVO fuel at EVC = −74 °CA and MAP = 160 kPa; (a) mid-load, (b) high-load. Note that for larger fuel quantity the y-axis scale is doubled.

mixture cooling. The expansion temperature is clearly below the polytrophic characteristics at this particular point.

Fig. 14 explains this behaviour by way of the NVO HRR analysis. For each operating point, a clear evaporative cooling effect is observed immediately after the fuel injection at −40 °CA. This effect is proportional to the NVO fuel quantity and is most apparent in Fig. 14b. Here, at elevated load, the following heat release from the oxidation is of the order of magnitude smaller than at the mid-load case, even though similar fuel quantities are applied for reforming. This correlates with the generally lower equivalence ratio of the high-load case. This observation is in line with the remarks made while comparing the air-path parameter sweep for both loads. Figs. 9 and 11 and the corresponding discussion provide more details.

Looking at the mid-load operating point in Fig. 14a, both the peak and cumulative HRR increase with the level of NVO fuelling. Most of the injected fuel can form a combustible mixture because there is sufficient oxygen in the recompressed gases, and the given ignition delay allows time for mixing. In the high-load case (Fig. 14b) the same phenomena is hampered by insufficient oxygen. Moreover, in the high-load case with the highest NVO fuelling (4.8 mg), evaporative cooling is so strong that it almost completely prohibits oxidation, resulting in overall negative NVO HRR. Fig. 13b shows that for this condition the peak NVO temperature drops below 1100 K because of fuel vaporization. This phenomenon also explains the insensitivity of λ and exhaust temperature while raising NVO fuel mass above 4 mg, as seen in Fig. 12.

At the higher IVO temperature associated with greater NVO fuelling (Fig. 13a), fresh air aspiration is reduced. This explains the reduction in overall mixture strength seen in Fig. 12. The resulting IVC mixture is not only richer, but with the EGR ratio unchanged, also significantly hotter due to the elevated temperature of residuals. This thermal effect is responsible for the accelerated combustion clearly visible on the main event pressure trace presented in Fig. 15a. The in-cylinder temperature traces presented in Fig. 16a, confirm this thermal effect: the compression part of the temperature trace for high NVO fuel quantities is significantly higher than it is with low fuel quantities. Note that the

thermal effect of fuel reforming, shown in Fig. 13a for higher NVO fuel quantities, is reinforced by correspondingly smaller amount of fuel injected along with SOI_2, giving less evaporative cooling of the mixture after IVO.

While the relationship between NVO and main event compression temperatures for the mid-load case is evident, the propagation of NVO thermal effect towards the IVC conditions for the high-load case is much more complex. Interestingly, at high-load with the greatest NVO fuel share (4.8 mg), despite extensive NVO cooling demonstrated in Fig. 14b, the temperature at end of compression apparently is higher than in other cases (Fig. 16b). This peculiar effect can be explained by the changes in the thermodynamic properties of the working fluid: the amount of NVO fuel affects the amount of aspirated air and trapped residuals that are close to stoichiometric point. Consequently, the EGR/λ trade-off has a meaningful effect on adiabatic exponent.

The higher end-of-compression temperatures in all cases translate into earlier auto-ignition, as evident in Fig. 16. Note that the chemical effects of NVO fuel-reforming also change ignition delay. These chemical effects will not be discussed in detail because it is the thermal ones that dominate [10].

In Figs. 15 and 16 it can be noted that for both engine-loads, expansion pressures and temperatures increase with the reduction of NVO fuel. The governing factor here is the amount of chemical energy delivered to the main combustion event. A rule of thumb is that the reduction of NVO fuel reduces the heat released during exhaust re-compression. This finally increases the energy input to the main cycle, translating directly to the exhaust temperature trend recorded in Fig. 12.

The HRR plots in Fig. 17 confirm the in-cylinder pressure-based observation that the ignition delay is shorter when NVO fuelling increases. The important remark is that combustion not only commences earlier but also is considerably faster. This observation introduces the following discussion about the effects of the investigated strategies on PRR.

3.3. The effect of investigated strategies on the PRR

The effects of NVO fuelling, EVC timing and MAP on PRR are shown in Fig. 18. It is noticeable that increasing the engine-load by approximately 30% from the baseline mid-load case (IMEP ≈ 0.58 MPa) almost doubles the PRR. The combustion harshness limit in terms of PRR_{max} at the examined engine-speed of 1500 rpm usually is considered to be at 0.6–0.7 MPa/°CA [18,48]. To get close to this requirement at high engine-load, only a very narrow calibration window can be used, operating at low split-ratios and applying very late EVC timing.

For the mid-load case, optimisation of PRR_{max} is possible within a large range of individual parameter settings: certain trends can be detected in Fig. 18a. Reduction in NVO fuelling generally reduces the PRR_{max}, as already indicated by reduced HRR signatures in Fig. 17. However, note that the trend is non-monotonic at a large split-ratio regime, where it is possible to comply with the adopted PRR_{max} limit by limiting the oxygen available for fuel-reforming. Either reducing the MAP or applying late EVC can be used to do this. Late EVC, as mentioned before, is also effective for the high-load case, enabling saturated PRR_{max} at a reduced level of 1.5 MPa/°CA, independently of the MAP level and despite elevated NVO fuelling.

Although the majority of the effects of investigated strategies on PRR can be qualitatively explained on the basis of fundamental-level analysis, as discussed in Sections 3.1 and 3.2, many results in Fig. 18 still seem not to follow any consistent trends. One example is the peculiar effect of MAP. Depending on the parameter combination and load conditions, an increase in boost pressure either increases or reduces PRR. Note that this observation actually echoes the situation described in this study's introductory literature review, citing conflicting reports from different sources on MAP's effect on PRR. The following discussion aims to synthesize the lessons learned through the detail analysis of the

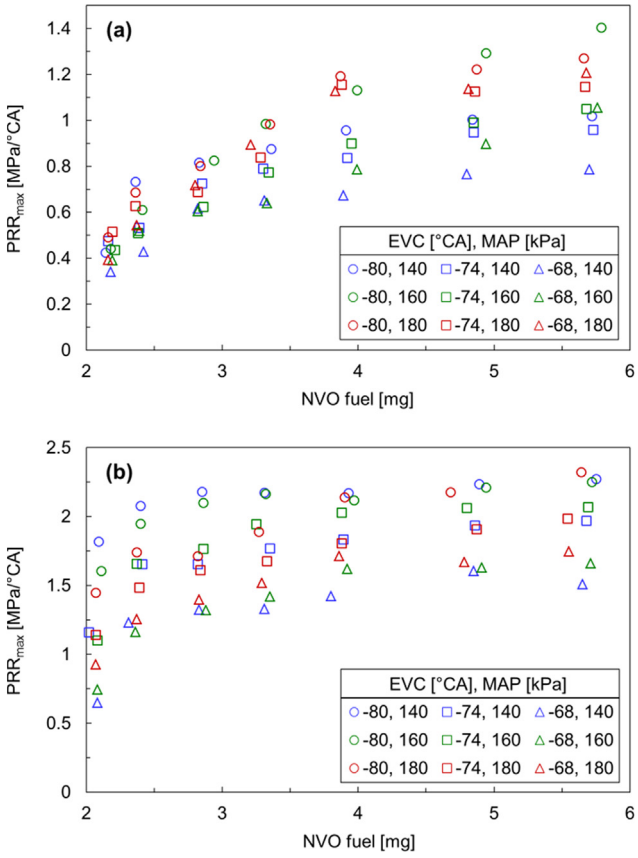

Fig. 18. PRR_{max} versus quantity of NVO fuel for all investigated conditions; (a) mid-load case, (b) high-load case.

thermal effects. This leads to Eq. (4) which puts them into perspective and provides a systematic explanation of the trends seen in Fig. 18.

The previous sections implied that higher NVO fuelling, through dominating thermal effects during NVO, causes both advanced combustion and shortened combustion duration. Fig. 19 verifies this thesis for the entire spectrum of tested parameter configurations. Here, CA50 is taken as the synthetic indicator for both combustion characteristics. According to Eq. (4), the CA50 is, at the same time, an important factor which indirectly (by means of in-cylinder volume) influences PRR. One can notice that Fig. 19 confirms the trend observed for specific points discussed in relation to Fig. 17, and (i) CA50 advances with increased fuel split ratio. The effects of air-path measures are also seen here and confirm the specific observations made in Section 3.1. Summarizing, Fig. 19 shows combustion advances both (ii) with earlier EVC and (iii) with increased MAP.

Regarding the magnitude of the above effects, it varies depending upon parameter configurations. For instance, NVO fuel variation has the biggest influence on the location of 50% MFB for cases with high MAP. This corresponds to high lambda enabling exothermic reactions as discussed in Section 3.2. According to the same mechanism, the magnitude of the MAP effect on the CA50 is greatest with elevated NVO fuelling. The magnitude of the EVC influence, on the other hand, remains majorly independent of both MAP and fuel split ratio.

Fig. 20 aims at decoupling the effect of individual parameters on combustion duration, which according to Eq. (4), directly impacts PRR. Note that qualitatively those effects are the same as for CA50 discussed in Fig. 19. Thus, it is possible to extend combustion duration either by reducing NVO fuelling and MAP or by applying the late EVC strategy. The quantitative effects are, however, considerably smaller. While the regulation window in CA50 is more than 15 °CA for the mid-load case (Fig. 20a), the corresponding effect in combustion duration is less than

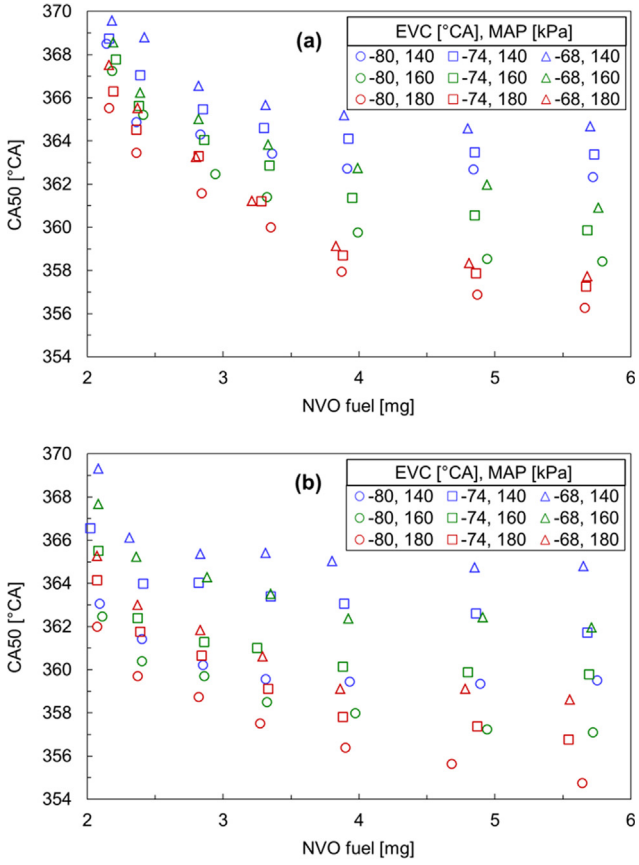

Fig. 19. CA50 versus quantity of NVO fuel for all investigated conditions; (a) mid-load case, (b) high-load case.

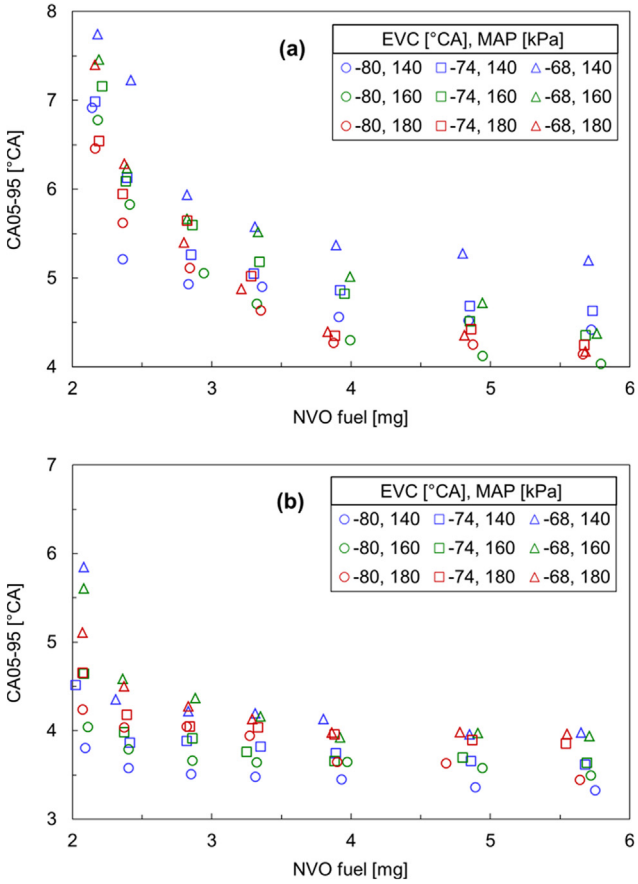

Fig. 20. Combustion duration versus quantity of NVO fuel for all investigated conditions; (a) mid-load case, (b) high-load case.

4 °CA (Fig. 18a). It should be noted, however, that in accordance to Eq. (4), PRR is much more sensitive to the reaction rate than to CA50. This is because CA50 affects PRR indirectly, i.e. with consideration of relatively small changes of cylinder volume. Nevertheless, the split ratio is highly relevant in terms of combustion duration, especially at high-boost conditions. Still, sensitivity to NVO fuelling is only attained for split ratios below 20% overall fuel energy. The insensitivity region is larger for the case with higher fuelling, as is evident in Fig. 20b. For the extreme setting of EVC at −80 °CA and lowest tested MAP of 140 kPa, the insensitivity effectively starts when raising the split ratio from around 8% to 10%. The narrow control window is attributed to the nearly stoichiometric mixture in this particular region.

Generally, analysis of Figs. 19 and 20 shows the effects of air-path parameters on both combustion indicators are not unambiguous in all cases. However, correlations of CA50 and combustion duration, demonstrated in Fig. 21, clearly show the cause and effect relationship that determines the influence of air-path and injection strategies on PRR levels. They show combustion duration is clearly correlated with combustion timing. For CA50 points located after TDC, the CA05-95 scales with in-cylinder volume. MAP clearly affects the offset of the characteristics, which is explainable through the effect of mixture strength on the reaction rates. Interestingly, MAP does not affect the slope. In contrast, when both fuel quantities are compared, higher load more than doubles the slope.

The linear trends observed in Fig. 21 appear solely if the 50% fuel's burn appears after top dead centre. Under these conditions the increase of volume reduces pressure and temperature, and thus extend combustion duration. For the set of points where CA50 appears before TDC, the combustion is accelerated by compression effect.

For the high-load case changing the NVO fuelling and the EVC timing mainly affects the start of combustion, with only slight effect on the duration. Note however, that in terms of the impact on PRR the latter factor has a profound effect. This is because combustion duration occurs directly in Eq. (4), while CA50 acts through in-cylinder volume, which changes relatively much less around TDC and is non-monotonic in this range.

Fig. 22 pulls the above discussion together by aligning the PRR_{max} with the denominator of Eq. (4). There is very good correlation between the mentioned parameters. At fixed fuel quantity and assuming that the adiabatic exponent is constant (compositional sensitivity of γ is very small), the trends should be linear. Instead, a non-linearity can be observed for both fuel quantities, and additionally there are some qualitative differences in the two PRR characteristics. However, common for both engine-load cases is the breaking points in the region, where CA50 appears near the TDC. These points are denoted by circles in Fig. 22. The shift of PRR towards higher values where CA50 is before TDC is especially noticeable for the high-load conditions (Fig. 22b), where typically combustion is more advanced. This indicates that there is large PRR_{max} sensitivity to volume change and also implies that the volume-change component in Eq. (2) cannot be completely neglected if high prediction accuracy is required.

To emphasize non-linearity of the trends more clearly, the PRR_{max} values predicted with the use of Eq. (4) are included in Fig. 22, denoted as $PRR_{1st\ law}$. It is noticeable that, at both engine-loads, the intersections of the theoretical end experimental values appear for conditions where CA50 ≈ TDC. The effect of the increasing change in volume as CA50 is delayed after TDC is clearly noticeable when the trend of $PRR_{1st\ law}$ line is compared with experimental linear fit to the points with CA50 located after TDC. The deviation of experimental trend from the theoretical line increases as the Eq. (4) denominator becomes smaller. It should be also noted that in spite of the effect of volume change there

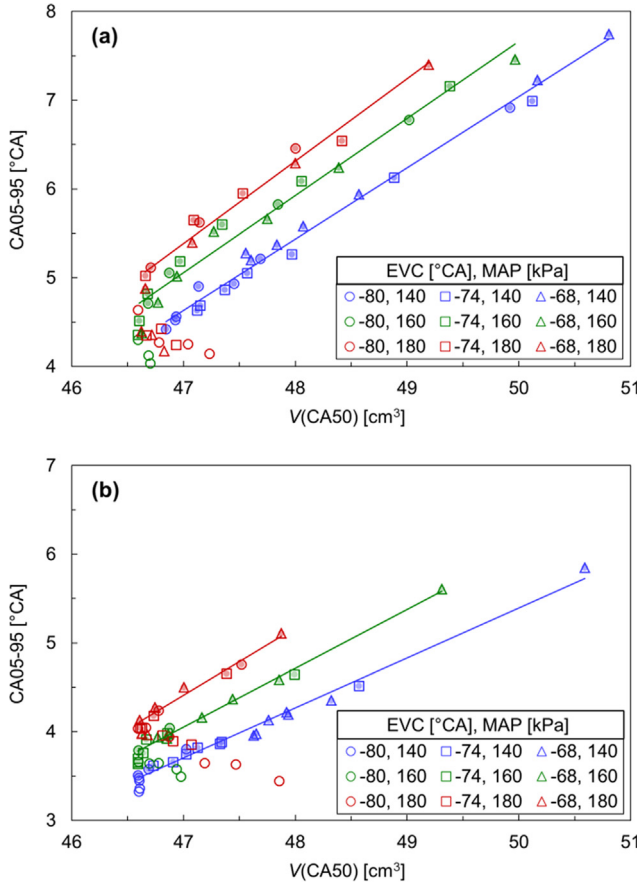

Fig. 21. Combustion duration versus volume at CA50 for all investigated conditions; (a) mid-load case, (b) high-load case. The filled points indicate cases with CA50 located after TDC. Trend lines are fitted solely to these sets of points.

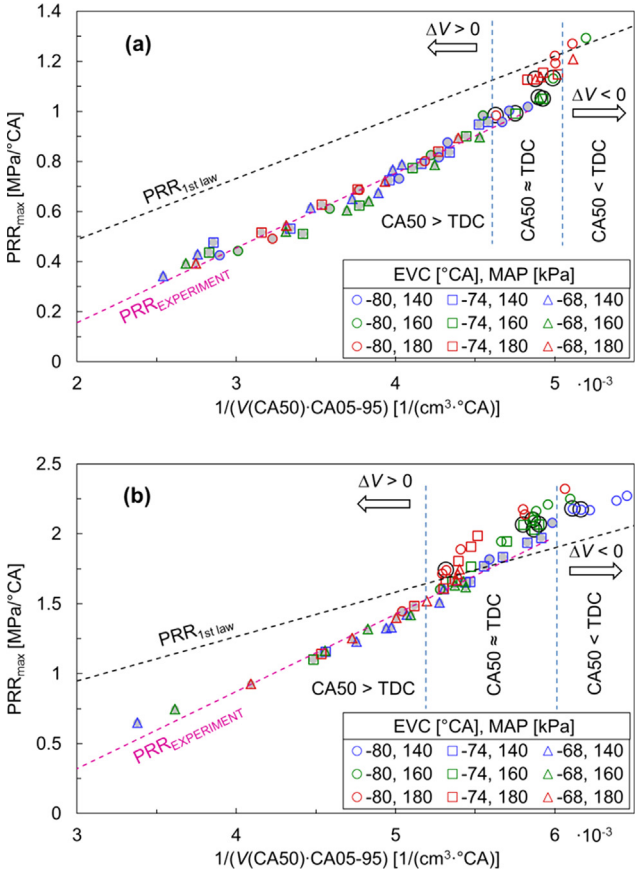

Fig. 22. PRR versus $1/(V(\mathrm{CA50})\cdot\mathrm{CA05\text{-}95})$ for all investigated conditions; (a) mid-load case, (b) high-load case. The $\mathrm{PRR_{1st\ law}}$ line is drawn using Eq. (4), assuming the constant m_F corresponding to the total fuel value of the considered load point (19 mg and 24 mg respectively for case (a) and (b)), and assuming constant $\gamma = 1.3$. The $\mathrm{PRR_{EXPERIMENT}}$ lines are fitted to shaded points with CA50 beyond TDC. Points surrounded by a circle are those near the TDC.

are also other factors affecting the discrepancy between real and predicted $\mathrm{PRR_{max}}$ values. It is enough to mention non-linear but sigmoidal MFB or neglected heat transfer.

Nevertheless, the main message from Figs. 21 and 22 is that when aiming at PRR control in a residual-affected HCCI engine the focus should not be on the effect of individual parameters. Bearing in mind that under all conditions CA50 should be located after TDC to optimise thermal efficiency, there is nearly a linear effect on $\mathrm{PRR_{max}}$ for a factor combining CA50 and combustion duration. One should note that slight deviations from this linearity stem from specifics of residual-affected HCCI engine operation. Specifically, the $\mathrm{PRR_{1st\ law}}$ lines in Fig. 22 are drawn using Eq. (4), assuming the constant m_F corresponding to the total fuel value of the considered load point. But the actual mass that affects PRR in Eq. (4) is always slightly lower because some of the fuel oxidizes during the NVO phase. The energy transferred to the main cycle depends on the split ratio and oxygen availability as discussed in Section 3.2. Thus, the deviations from linearity at low $\mathrm{PRR_{max}}$ regime indicate different amounts of energy delivered to the main event.

3.4. Outlook on applicability and trade-offs

Closed-loop control has already proven to be necessary for efficient HCCI operation. Various techniques have been demonstrated to facilitate this, such as fast thermal management [49] or VVA [50]. Importantly, Jung and Iida [51] applied external and rebreathed EGR, arguing that they can be successfully used to control pressure-rise rates at high-load operational boundary. Ultimately, most of these control techniques use CA50 as a feedback variable due to its direct relationship with IMEP and efficiency, and because there is established methodology for real-time calculation from on-board in-cylinder pressure measurement. While residually affected HCCI with NVO direct injection provides significant advantages over the conventional PVO concept in terms of both low- and high-load extension potential, it also greatly adds to the complexity. This is the reason why multi-input, PRR-oriented control has not been demonstrated for residually affected HCCI with NVO fuel injection. However, this study implies that various measures explored for PRR mitigation, despite their complex governing mechanisms (see Sections 3.1 and 3.2), can be narrowed down to just two main parameters when PRR control is considered. The study indicates that in the applicable operational region, $\mathrm{PRR_{max}}$ estimation can be linearized using only the volume at CA50 and combustion duration, no matter which mitigation measure is used. Furthermore, correlations between both these parameters, shown in Fig. 21, provide background to reduce the input data to just one combustion timing parameter: CA50. It should be noted, however, that quantification of this correlation would be individual for a given engine and its air-path conditions and so should be modelled accordingly.

Fig. 18 clearly shows that reducing NVO fuel quantity is the primary strategy when considering $\mathrm{PRR_{max}}$ mitigation in pursuit of HCCI regime extension. At high engine-loads the recirculated exhaust is already much hotter than at low-load operation. Therefore it requires less NVO treatment through fuel reforming to secure the proper combustion onset as shown in Fig. 19. Moreover, lowering NVO fuelling is advantageous from the perspective of net indicated efficiency combined with a reducing effect on $\mathrm{NO_X}$ emissions [52]. During the reforming at NVO, the heat is released under considerably lower apparent

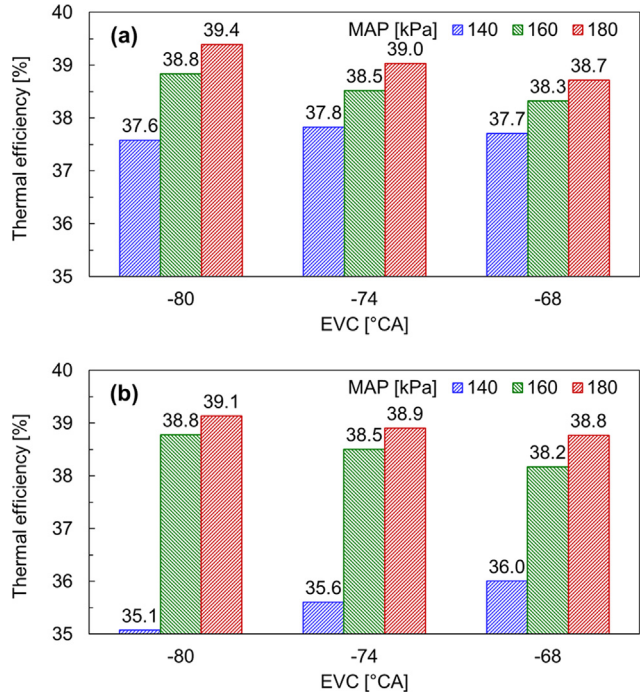

Fig. 23. Indicated thermal efficiency for approximately 2 mg of NVO fuel; (a) mid-load case, (b) high-load case.

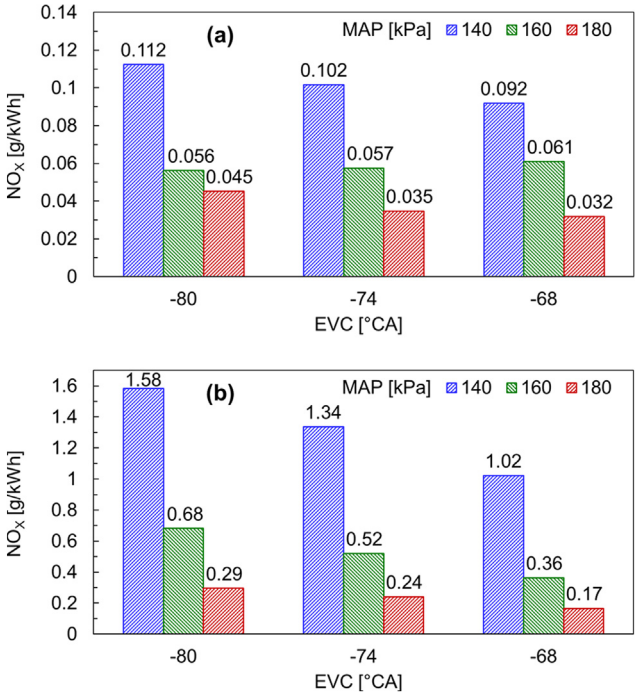

Fig. 24. Indicated specific NO_X emissions for approximately 2 mg of NVO fuel; (a) mid-load case, (b) high-load case. Note that for the high-load case the y-axis scale is more than an order of magnitude greater than for the mid-load.

compression ratios and with a short expansion phase, making the process far less efficient than the main event in terms of producing work. Thus, the lower the amount of NVO fuel, the lower the reformation losses. Since there is no trade-off between PRR_{max}, efficiency and NO_X here, the effects of fuel split ratio on the two latter parameters will not be discussed here. For details on efficiency and emissions with different NVO injection strategies, the reader is referred to the earlier works by the authors [10,46].

Figs. 23 and 24 show how the net indicated efficiency and NO_X emissions are affected by different air-path strategies. This is demonstrated for the lowest stable NVO fuelling of 2 mg because this particular setting enables PRR_{max} mitigation below the assumed limit of 0.7 MPa/°CA at excessive loads of 0.75 MPa (Fig. 18).

Retarding the EVC has a significant potential in reducing PRR, especially with high-load operation (Fig. 22). Fig. 23 indicates this does not majorly affect efficiency. This is because the efficiency loss from retarded and elongated combustion (which ultimately enables lower PRR_{max}), is compensated with elongated expansion. The strategy also remains neutral in terms of emissions, in most cases contributing to lower NO_X through reduced combustion temperatures, as shown in Fig. 24.

The boost pressure has a profound effect on CA50, providing significantly retarded combustion onset with low MAP, demonstrated in Fig. 19. Interestingly, this does not translate into reduced PRR_{max} levels when compared to other MAP settings (Fig. 18) because the combustion duration gets reduced significantly (Fig. 21). While the reasons for this are elaborated in-depth in Section 3.1, at this point it is important to note that both the retarded combustion and lower lambda cause a significant deterioration in efficiency. This is clearly seen in Fig. 23b. The lower lambda has an even greater effect on NO_X. Fig. 24 shows that NO_X emissions on average double with MAP reduction from 160 MPa to 140 MPa. Without detail discussion about the actual numbers relating to efficiency loss and NO_X emissions, Fig. 18 shows that PRR_{max} reduction with reduced MAP is only possible when combined with the latest possible exhaust valve timing. Taking into account the heavy trade-off indicated in Figs. 23 and 24, this strategy should be used as a last possible measure and applied only when both EVC retardation and NVO fuel quantity minimization have reached their limits due to misfire. Note also that practical application of introducing high MAP carries an additional penalty because supercharging, considered advantageous for NVO HCCI due to combustion stability, requires additional power that impacts overall engine efficiency.

4. Conclusions

The hypothesis states that irrespective of the governing mechanisms' complexities, every individual strategy for pressure rise rate mitigation can be narrowed down to its effect on combustion phasing. The study's validation tests reveal that the straightforward route towards pressure rise rate reduction is delay of combustion onset and simultaneous reduction of combustion rate. Results show that, in the operating range of combustion onsets, which are feasible for acceptable efficiency, both combustion onset and combustion rate are closely coupled to each other with linear correlation.

This study indicates that multi-parameter, pressure rise rate control in residually affected HCCI engine is feasible. This could be applied as a form of supervisory control, extending the high-load operating range at elevated fuelling. The results also outline how to formulate such a control strategy, which should be based on actual trade-offs between pressure rise rate on one side and efficiency and emissions on the other.

Reducing fuel injected during negative valve overlap (for reforming) is the primary strategy when considering pressure rise mitigation for HCCI regime extension. At high loads the recirculated exhaust is already much hotter than at low loads, requiring less treatment through fuel reforming for proper combustion onset. Furthermore, as long as negative valve overlap is considered as an enabler for HCCI, diminishing the trapped residuals and reducing fuel injected for reforming, applied as pressure rise control measures, do not suffer from trade-offs that harm efficiency and emissions.

Reducing boost pressure shortens, or at least is neutral towards, combustion duration, but clearly retards combustion onset. Thus, it has a less profound impact on pressure rise rate than does the variable exhaust valve actuation, because the two combustion indicators, onset

and duration, act against each other. Low boost-pressure operation harms efficiency and greatly increases nitrogen oxides emissions.

There are a handful of additional conclusions that help fill some knowledge gaps:

- The qualitatively different reaction to boost pressure in terms of combustion onset and duration explains earlier studies' inconsistencies regarding the effect of boost on pressure rise rate. At some conditions, determined by specific effects of λ on fuel reforming, the effect of combustion duration dominates the usually prevailing effect of volume change, thus changing how boost affects pressure rise rates.
- Regarding the peak-pressure rise rate estimation method proposed, the volume change component cannot be neglected if to-the-point accuracy is required. Its effect is, however, secondary to the combustion indicators, so for control purposes can be neglected in favour of using a constant correction on linearization based on crank angle of 50% mass burnt. For combustion onsets after top dead centre, due to change in monotony, volume change is responsible for significant deviation from linearity.
- Additional peak pressure rise rate estimation uncertainty arises because of the differences in main-cycle fuel energy density. This stems from different oxidation rates during negative valve overlap. As far as this effect is traceable using thermodynamic analysis, it is difficult to consider it in control actions.

Acknowledgments

The research was financed in the framework of the project Lublin University of Technology (Poland) – Regional Excellence Initiative, funded by the Polish Ministry of Science and Higher Education (contract No. 030/RID/2018/19).

References

[1] Reitz RD, Duraisamy G. Review of high efficiency and clean reactivity controlled compression ignition (RCCI) combustion in internal combustion engines. Prog Energy Combust Sci 2015;46:12–71. https://doi.org/10.1016/j.pecs.2014.05.003.
[2] Lavy J, Dabadie J-C, Angelberger C, Duret P, Willand J, Juretzka A, et al. Innovative ultra-low NOx controlled auto-ignition combustion process for gasoline engines: the 4-SPACE project. SAE Technical Paper 2000-01-1837; 2000. doi: 10.4271/2000-01-1837.
[3] Kumar P, Rehman A. Bio-diesel in homogeneous charge compression ignition (HCCI) combustion. Renew Sustain Energy Rev 2016;56:536–50. https://doi.org/10.1016/j.rser.2015.11.088.
[4] Sjöberg M, Dec JE, Cernansky NP. Potential of thermal stratification and combustion retard for reducing pressure-rise rates in HCCI engines, based on multi-zone modeling and experiments. SAE Technical Paper 2005-01-0113; 2005. doi: 10.4271/2005-01-0113.
[5] Saxena S, Bedoya ID. Fundamental phenomena affecting low temperature combustion and HCCI engines, high load limits and strategies for extending these limits. Prog Energy Combust Sci 2013;39:457–88. https://doi.org/10.1016/j.pecs.2013.05.002 Review.
[6] Valero-Marco J, Lehrheuer B, López JJ, Pischinger S. Potential of water direct injection in a CAI/HCCI gasoline engine to extend the operating range towards higher loads. Fuel 2018;231:317–27. https://doi.org/10.1016/j.fuel.2018.05.093.
[7] Agarwal AK, Singh AP, Maurya RK. Evolution, challenges and path forward for low temperature combustion engines. Prog Energy Combust Sci 2017;61:1–56. https://doi.org/10.1016/j.pecs.2017.02.001.
[8] Zhou L, Hua J, Liu F, Liu F, Feng D, Wei H. Effect of internal exhaust gas recirculation on the combustion characteristics of gasoline compression ignition engine under low to idle conditions. Energy 2018;164:306–15. https://doi.org/10.1016/J.ENERGY.2018.08.109.
[9] Olesky LM, Lavoie GA, Assanis DN, Wooldridge MS, Martz JB. The effects of diluent composition on the rates of HCCI and spark assisted compression ignition combustion. Appl Energy 2014;124:186–98. https://doi.org/10.1016/J.APENERGY.2014.03.015.
[10] Hunicz J, Mikulski M. Investigation of the thermal effects of fuel injection into retained residuals in HCCI engine. Appl Energy 2018;228:1966–84. https://doi.org/10.1016/j.apenergy.2018.07.075.
[11] Liu H, Ma G, Ma N, Zheng Z, Huang H, Yao M. Effects of charge concentration and reactivity stratification on combustion and emission characteristics of a PFI-DI dual injection engine under low load condition. Fuel 2018;231:26–36. https://doi.org/10.1016/j.fuel.2018.05.027.
[12] Zhou L, Dong K, Hua J, Wei H, Chen R, Han Y. Effects of applying EGR with split injection strategy on combustion performance and knock resistance in a spark assisted compression ignition (SACI) engine. Appl Therm Eng 2018;145:98–109. https://doi.org/10.1016/J.APPLTHERMALENG.2018.09.001.
[13] Fatouraie M, Wooldridge M. Optical investigation of the effects of ethanol/gasoline blends on spark-assisted HCCI. J Eng Gas Turbines Power 2014;136:081507https://doi.org/10.1115/1.4026862.
[14] Li J, Zhao H, Ladommatos N, Ma T. Research and development of controlled auto-ignition (CAI) combustion in a 4-stroke multi-cylinder gasoline engine. SAE Technical Paper 2001–01-3608 2001. https://doi.org/10.4271/2001-01-3608.
[15] Ma H, Xu H, Wang J, Tan C. Investigation on the self-stabilization feature of HCCI combustion. SAE Technical Paper 2014–01-2663 2014. https://doi.org/10.4271/2014-01-2663.
[16] Hunicz J. Cycle-by-cycle variations in autonomous and spark assisted homogeneous charge compression ignition combustion of stoichiometric air–fuel mixture. Int J Spray Combust Dyn 2018;10:231–43. https://doi.org/10.1177/1756827718763564.
[17] Gorzelic P, Shingne P, Martz J, Stefanopoulou A, Sterniak J, Jiang L. A low-order adaptive engine model for SI-HCCI mode transition control applications with cam switching strategies. Int J Engine Res 2016;17:451–68. https://doi.org/10.1177/1468087415585016.
[18] Scaringe R, Wildman C, Cheng WK. On the high load limit of boosted gasoline HCCI engine operating in NVO mode. SAE Int J Engines 2010;3:35–45. https://doi.org/10.4271/2010-01-0162.
[19] Kulzer A, Lejsek D, Nier T. A thermodynamic study on boosted HCCI: motivation, analysis and potential. SAE Int J Eng 2010;3:733–49. https://doi.org/10.4271/2010-01-1082.
[20] Kulzer A, Nier T, Karrelmeyer R. A thermodynamic study on Boosted HCCI experimental results. SAE Technical Paper 2011–01-0905 2011. https://doi.org/10.4271/2011-01-0905.
[21] Dec JE, Yang Y. Boosted HCCI for high power without engine knock and with ultra-low NOx emissions - using conventional gasoline. SAE Int J Engines 2010;3:750–67. https://doi.org/10.4271/2010-01-1086.
[22] Yap D, Wyszynski ML, Megaritis A, Xu H. Applying boosting to gasoline HCCI operation with residual gas trapping. SAE Technical Paper 2005–01-2121 2005. https://doi.org/10.4271/2005-01-2121.
[23] Canakci M. Combustion characteristics of a DI-HCCI gasoline engine running at different boost pressures. Fuel 2012;96:546–55. https://doi.org/10.1016/j.fuel.2012.01.042.
[24] Shingne PS, Middleton RJ, Borgnakke C, Martz JB. The effects of boost pressure on stratification and burn duration of gasoline homogeneous charge compression ignition combustion. Int J Engine Res 2018;146808741775417. https://doi.org/10.1177/1468087417754177.
[25] Dec JE, Yang Y, Dronniou N. Boosted HCCI - controlling pressure-rise rates for performance improvements using partial fuel stratification with conventional gasoline. SAE Int J Engines 2011;4:1169–89. https://doi.org/10.4271/2011-01-0897.
[26] Turkcan A, Ozsezen AN, Canakci M. Effects of second injection timing on combustion characteristics of a two stage direct injection gasoline-alcohol HCCI engine. Fuel 2013;111:30–9. https://doi.org/10.1016/j.fuel.2013.04.029.
[27] Turkcan A, Altinkurt MD, Coskun G, Canakci M. Numerical and experimental investigations of the effects of the second injection timing and alcohol-gasoline fuel blends on combustion and emissions of an HCCI-DI engine. Fuel 2018;219:50–61. https://doi.org/10.1016/j.fuel.2018.01.061.
[28] Hunicz J, Tmar A, Krzaczek P. Effects of mixture stratification on combustion and emissions of boosted controlled auto-ignition engines. Energies 2017;10:2172. https://doi.org/10.3390/en10122172.
[29] Yang Dbo, Wang Z, Wang JX, Shuai Sjin. Experimental study of fuel stratification for HCCI high load extension. Appl Energy 2011;88:2949–54. https://doi.org/10.1016/j.apenergy.2011.03.004.
[30] Kodavasal J, Lavoie GA, Assanis DN, Martz JB. The effect of diluent composition on homogeneous charge compression ignition auto-ignition and combustion duration. Proc Combust Inst 2015;35:3019–26. https://doi.org/10.1016/j.proci.2014.06.152.
[31] Splitter DA, Reitz RD. Fuel reactivity effects on the efficiency and operational window of dual-fuel compression ignition engines. Fuel 2014;118:163–75. https://doi.org/10.1016/j.fuel.2013.10.045.
[32] Benajes J, García A, Monsalve-Serrano J, Boronat V. Achieving clean and efficient engine operation up to full load by combining optimized RCCI and dual-fuel diesel-gasoline combustion strategies. Energy Convers Manage 2017. https://doi.org/10.1016/j.enconman.2017.01.010.
[33] Pedrozo VB, Zhao H. Improvement in high load ethanol-diesel dual-fuel combustion by Miller cycle and charge air cooling. Appl Energy 2018;210:138–51. https://doi.org/10.1016/j.apenergy.2017.10.092.
[34] Mikulski M, Bekdemir C. Understanding the role of low reactivity fuel stratification in a dual fuel RCCI engine – a simulation study. Appl Energy 2017;191:689–708. https://doi.org/10.1016/j.apenergy.2017.01.080.
[35] Mikulski M, Balakrishnan PR, Doosje E, Bekdemir C. Variable valve actuation strategies for better efficiency load range and thermal management in an RCCI engine. SAE Technical Paper 2018–01-0254 2018. https://doi.org/10.4271/2018-01-0254.
[36] Asai G, Watanabe Y, Ishiguro S, Shibata G, Ogawa H, Kobashi Y. Chemical reaction processes of fuel reformation by diesel engine piston compression of rich homogeneous air-fuel mixture. SAE Int J Engines 2017;10:2624–35.
[37] Yu W, Xie H, Chen T, Li L, Song K, Zhao H. Effects of active species in residual gas on auto-ignition in a HCCI gasoline engine. SAE Technical Paper 2012–01-1115 2012. https://doi.org/10.4271/2012-01-1115.
[38] Xie H, Lu J, Chen T, Li L, Li C, Zhao H. Chemical effects of the incomplete-oxidation

products in residual gas on the gasoline HCCI auto-ignition. Combust Sci Technol 2014;186:273–96. https://doi.org/10.1080/00102202.2013.858714.
[39] Puranam SV, Steeper RR. The effect of acetylene on iso-octane combustion in an HCCI engine with NVO. SAE Int J Engines 2012;5:1551–60. https://doi.org/10.4271/2012-01-1574.
[40] Wolk B, Ekoto I, Northrop WF, Moshammer K, Hansen N. Detailed speciation and reactivity characterization of fuel-specific in-cylinder reforming products and the associated impact on engine performance. Fuel 2016;185:341–61. https://doi.org/10.1016/j.fuel.2016.07.103.
[41] Ekoto IW, Wolk BM, Northrop WF, Hansen N, Moshammer K. Tailoring charge reactivity using in-cylinder generated reformate for gasoline compression ignition strategies. J Eng Gas Turbines Power 2017;139:122801https://doi.org/10.1115/1.4037207.
[42] Hunicz J, Mikulski M, Rybak A. Combustion and emissions of controlled auto-ignition engine under stratified mixture conditions. IOP Conf Ser: Mater Sci Eng 2018;421. https://doi.org/10.1088/1757-899X/421/4/042028.
[43] Hunicz J, Mikulski M, Geca MS, Kordos P, Komsta H. Late direct fuel injection for reduced combustion rates in a gasoline controlled auto-ignition engine. Therm Sci 2018;22:1299–309. https://doi.org/10.2298/TSCI180224145H.
[44] Hunicz J, Kordos P. Experimental study of the gasoline engine operated in spark ignition and controlled auto-ignition combustion modes. SAE Technical Paper 2009–01-2667 2009. https://doi.org/10.4271/2009-01-2667.
[45] Hunicz J, Geca MS, Kordos P, Komsta H. An experimental study on a boosted gasoline HCCI engine under different direct fuel injection strategies. Exp Therm Fluid Sci 2015;62:151–63. https://doi.org/10.1016/j.expthermflusci.2014.12.014.
[46] Hunicz J. An experimental study of negative valve overlap injection effects and their impact on combustion in a gasoline HCCI engine. Fuel 2014;117:236–50. https://doi.org/10.1016/j.fuel.2013.09.079.
[47] Hunicz J. An experimental study into the chemical effects of direct gasoline injection into retained residuals in a homogeneous charge compression ignition engine. Int J Engine Res 2016;17:1031–44. https://doi.org/10.1177/1468087416636492.
[48] Eng JA. Characterization of pressure waves in HCCI Combustion. SAE Technical Paper 2002–01-2859 2002. https://doi.org/10.4271/2002-01-2859.
[49] Haraldsson G, Tunestål P, Johansson B, Hyvönen JHCCI. Closed-loop combustion control using fast thermal management. SAE Technical Paper 2004–01-0943 2004. https://doi.org/10.4271/2004-01-0943.
[50] Agrell F, Ångström H-E, Eriksson B, Wikander J, Linderyd J. Integrated simulation and engine test of closed loop HCCI control by aid of variable valve timings. SAE Technical Paper 2003–01-074 2003. https://doi.org/10.4271/2003-01-0748.
[51] Jung D, Iida N. Closed-loop control of HCCI combustion for DME using external EGR and rebreathed EGR to reduce pressure-rise rate with combustion-phasing retard. Appl Energy 2015;138:315–30. https://doi.org/10.1016/j.apenergy.2014.10.085.
[52] Hunicz J, Mikulski M. Application of variable valve actuation strategies and direct gasoline injection schemes to reduce combustion harshness and emissions of boosted HCCI engine. J Eng Gas Turbines Power 2019;141:071023https://doi.org/10.1115/1.4043418.